Acta Derm Venereol 2016; 96: 303–308

See also In-this-Issue, p. 291

INVESTIGATIVE REPORT

Skin Lamellar Bodies are not Discrete Vesicles but Part of a Tubuloreticular Network

Lianne DEN HOLLANDER[1], HongMei HAN[1,2], Matthijs DE WINTER[3], Lennart SVENSSON[4], Sergej MASICH[1], Bertil DANE-HOLT[1] and Lars NORLÉN[1,5]*

[1]Department of Cell and Molecular Biology (CMB), Karolinska Institutet, Stockholm, Sweden, [2]Max-Planck-Institut für molekulare Physiologie, Systemic Cell Biology, Dortmund, Germany, [3]Biomolecular Imaging, Faculty of Science, Utrecht University, Utrecht, The Netherlands, [4]Centre for Image Analysis, Uppsala University, Uppsala, and [5]Dermatology Clinic, Karolinska University Hospital, Stockholm, Sweden

Improved knowledge of the topology of lamellar bodies is a prerequisite for a molecular-level understanding of skin barrier formation, which in turn may provide clues as to the underlying causes of barrier-deficient skin disease. The aim of this study was to examine the key question of continuity vs. discreteness of the lamellar body system using 3 highly specialized and complementary 3-dimensional (3D) electron microscopy methodologies; tomography of vitreous sections (TOVIS), freeze-substitution serial section electron tomography (FS-SET), and focused ion beam scanning electron microscopy (FIB-SEM) tomography. We present here direct evidence that lamellar bodies are not discrete vesicles, but are part of a tubuloreticular membrane network filling out the cytoplasm and being continuous with the plasma membrane of stratum granulosum cells. This implies that skin barrier formation could be regarded as a membrane folding/unfolding process, but not as a lamellar body fusion process. ***Key words: skin barrier; CEMOVIS; TOVIS; FS-SET; FIB-SEM.***

Accepted Sep 30, 2015; Epub ahead of print Oct 6, 2015

Acta Derm Venereol 2016; 96: 303–308.

Lars Norlén, Department of Cellular and Molecular Biology (CMB), Karolinska Institutet, von Euler's v 1, SE-171 77 Stockholm, Sweden. E-mail: lars.norlen@ki.se

The body's barrier against water loss via evaporation and against penetration of certain exogenous substances is constituted by lipids that fill the extracellular space of the skin's surface layer, the stratum corneum (SC). These lipids have a unique molecular architecture, being organized as stacked bilayers of fully extended ceramides, with cholesterol associated with the ceramide sphingoid moiety (1).

Several skin diseases, such as eczema, psoriasis and the ichthyoses, are characterized by a deficient barrier function. Perturbed skin barrier formation may thus be an aetiological factor in barrier-deficient skin disease (2).

The formation of the skin barrier depends on deposition of lipids into the extracellular space between the viable and cornified epidermis (3). Prior to deposition, the lipids are located to, and delivered by, a membrane-bound organelle system termed the lamellar body system (synonyms: lamellar granules, membrane coating granules, Odland bodies (3–11)). Two models have been proposed for skin barrier formation; the Landmann model (8) and the membrane-folding model (12). The fundamental difference between the 2 models is that the Landmann model proposes that the lamellar body system is constituted by a multitude of discrete vesicles, while the membrane-folding model proposes that it is constituted by a single and coherent tubuloreticular membrane network. The Landmann model advocates that the physiological process underlying skin barrier formation belongs to the group of diffusion/fusion processes, like that of, for example, synaptic vesicle fusion (13), while the membrane-folding model infers that lipid secretion into the extracellular space takes place via unfolding of invaginations of the stratum granulosum (SG) cell plasma membrane. The seemingly discrete lamellar bodies seen in 2-dimensional (2D) electron micrographs are, according to the membrane-folding model, merely 2D projections of a single tubuloreticular membrane network. The lamellar bodies are thus not discrete vesicular structures, but are continuous with each other and with the plasma membrane, which in turn would profoundly affect the chemical and physical processes controlling skin barrier formation (12).

In this study, the discreteness vs. continuity of the lamellar body system was directly addressed using 3 different highly specialized and complementary 3D electron microscopy methodologies: tomography of vitreous sections (TOVIS) (14–16), freeze-substitution serial section electron tomography (FS-SET), and focused ion beam scanning electron microscopy (FIB-SEM) tomography (17), using cryo-electron microscopy of vitreous sections (CEMOVIS) (18–22) as a near-native high-resolution 2D reference.

MATERIALS AND METHODS

A more detailed description of experimental procedures is given in Appendix S1[1].

[1]https://doi.org/10.2340/00015555-2249

All human studies were approved by the authors' Institutional Review Board and followed the protocols of the Declaration of Helsinki. All subjects gave their written informed consent.

Skin biopsies (~$1.0 \times 1.0 \times 0.2$ mm^3) were taken from the volar forearm of 5 Caucasian males (median age 47 years; age range 40–57 years old) with no history of skin disease themselves or among first-degree relatives. The samples were immediately vitrified using a Leica EMPACT2 high-pressure freezer (Leica, Vienna, Austria) and cryosectioned at –140°C.

CEMOVIS images were recorded at –180°C with a Philips CM200 FEG electron microscope (Philips, Eindhoven, The Netherlands) equipped with a cooled slow scan 2,048 × 2,048 TVIPS TemCam-F224 HD CCD camera (pixel size 24 µm) at magnifications between 15,000 and 88,000, at a defocus between –0.5 µm and –3 µm, and with an electron dose between 3,000 and 3,000 e^-/nm^2.

TOVIS tilt series ($n = 7$) from 60° to –60° with 1° increment (i.e. each tilt-series containing 120 images), were recorded at a defocus of –2 µm under low-dose conditions (in total approximately 4,000 e^-/nm^2 per 120 image tilt-series) at a magnification of 20,000 on an area of approximately 1,600 × 1,700 nm^2. Tomographic 3D-reconstruction by weighted back-projection, low-pass filtering to 15 Ångström and segmentation, were performed with the IMOD software package (28).

Five sequential FS-TEM dual-axis tomograms, each composed of 240 images, were collected from 70° to –70° tilt, with a magnification of 20,000 and a defocus of –0.5 µm, from an area of approximately 1,700 × 1,600 nm^2. The combined serial section tomogram was then visualized by isosurface rendering, with the grey level set by using CEMOVIS post-tomography micrographs obtained at zero tilt angle from the same section area, as an internal reference. Membrane structures connected in 3D were segmented out using watershed segmentation (29). Isosurface rendering and segmentation were done in USCF Chimera (30).

Three FS-FIB-SEM data-sets were collected in 3 different areas from 2 skin samples using a FEI Nova Nanolab600 Dualbeam (FEI, Eindhoven, The Netherlands). Imaging was performed using a 2,000 eV beam (0.21 nA) with a pixel size of 3.57 nm. For each data-set, approximately 50 cross-sections were viewed with a dwell time of 60 µs. The stack of 50 2D images created with FS-FIB-SEM was combined into a single 3D volume using ImageJ (31) with the TomoJ plug-in and manually aligned with IMOD (28). Lanczos re-sampling (32) was used to lower the resolution of the aligned image stack. The re-sampled volume was visualized using isosurface rendering. The settings for the grey level were determined by measuring an easily distinguishable feature, like a lamellar body, in the original 2D image. The same feature in the reconstructed 3D volume was made to fit the corresponding features in the original 2D images by setting correctly the grey-scale intensity value. All the connected features were segmented using watershed segmentation. Both the isosurface rendering and segmentation were done in UCSF Chimera (30).

RESULTS

Cryo-electron microscopy of vitreous sections

In total more than 300 CEMOVIS micrographs of the interface between viable and cornified epidermis were obtained from the forearm and abdominal skin of 5 Caucasian males in their 40s and 50s with no history of skin disease.

For an account of the general ultrastructure of the interface between the SG and the SC, see (18, 22). Fig. 1 shows that apparent active sites of skin barrier formation were constituted by lamellar bodies and associated complex membrane structures, corresponding with data earlier reported (18). Lamellar bodies (Fig. 1; inset) were highly heterogeneous with respect to size, shape and interior electron-density patterns. They contained lamellar material, multigranular material and complex material in varying proportions. No clear demarcation was observed between lamellar, multigranular and complex material.

Fig. 1. Cryo-electron microscopy of vitreous sections (CEMOVIS) electron density map of the interface between viable and cornified epidermis. Multiple apparent active sites of skin barrier formation (*black boxes*) can be seen, constituted by lamellar bodies (*white asterisk*) and associated complex membrane structures (*black asterisk*). Lamellar bodies (*white asterisk*; inset) contain lamellar material (*inset white arrow*), multigranular material (*inset black arrow*) and complex material (*inset white-lined black arrow*) in varying proportions. *White dotted line* marks the interface between viable and cornified epidermis. *Inset*: enlarged view of lamellar body; SC: stratum corneum; SG: stratum granulosum; *Black-lined white arrows*: widened areas of the extracellular space; *Open black arrow*: cryo-section cutting direction; Section thickness: 50 nm; Defocus: –2 µm; *Scale bar*: 500 nm; *Inset scale bar*: 100 nm.

Highly heterogeneous membrane material, similar to the content of lamellar bodies, was found associated with invaginations of the plasma membrane in widened areas of the extracellular space between SG and SC (see Fig. 1).

TransGolgi networks were identified in association with lamellar bodies (Fig. S1A[1]) and in association with the extracellular space (Fig. S1B[1]) at the interface between the SG and the SC.

Tomography of vitreous sections

For the best view of the 3D-reconstructed TOVIS data we refer the reader to Movie SI[1] TOVIS.avi.

In total, 3 near-native skin sample volumes of approximately 1,000 × 500×50 nm^3 were 3D-reconstructed.

In the 3D-reconstructed TOVIS data, sections of tubules were omnipresent, while no vesicular structures were identified in any TOVIS data-set.

Membrane continuity between the cell plasma membrane and lamellar bodies and between lamellar bodies themselves was identified (best visualized in Movie SI[1] TOVIS. avi) (Fig. 2; Fig. S2[1]; Movie SI[1] TOVIS.avi).

The median diameter of the connections was 40.5 nm (range 3–90 nm; $n = 8$). Connections were not observed between all identified lamellar body sections in the 3D-reconstructed 50-nm thick skin sample sections. No discrete lamellar body structures were observed in any 3D-reconstructed sample. All lamellar bodies were represented as tubular sections with varying tubular diameters (Fig. 2C).

TransGolgi networks were, as for the CEMOVIS (Fig. S1A[1]) and the FS-SET (Fig. S1C[1]) data, identified in the TOVIS data (Fig. S1B[1]). Due to the limited thickness (approximately 50 nm) of the observable reconstructed 3D volume using high-resolution TOVIS, we were not able to obtain 3D-reconstructions containing both a transGolgi network and the adjacent plasma membrane concomitantly.

Stacked lamellar material with a lamellar periodicity of approximately 5 nm was resolved in the extracellular space and inside the lamellar body system in the TOVIS 3D-reconstructions (Fig. 2C). Multi-granular material associated with the stacked lamellar material observed in CEMOVIS 2D micrographs inside lamellar bodies and inside the adjacent extracellular space between viable and cornified epidermis (18, 22) (see Fig. 1; Fig S1A[1]) was not resolved in the TOVIS 3D-reconstructions.

Freeze-substitution serial section electron tomography

For the best view of the 3D-reconstructed FS-SET data we refer the reader to Movie SII[1] FS_SET. mov. A skin sample volume of approximately 1,500 × 1,500 × 400 nm^3, consisting of 5 individual stacked sequential sample volumes of approximately 1,500 × 1,500 × 80 nm^3 each, was 3D-reconstructed.

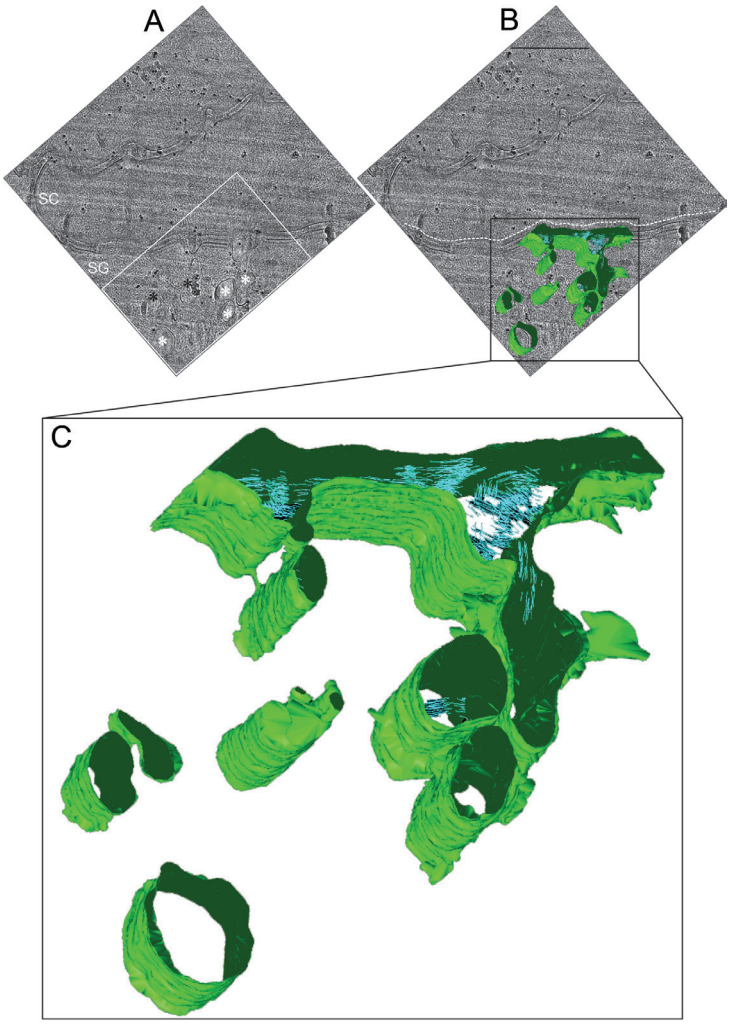

Fig. 2. Fifty nanometre thick tomography of vitreous sections (TOVIS) 3D-reconstruction of the interface between viable and cornified epidermis (see Movie SI[1] TOVIS.avi). (A) Post-tilt series zero-tilt TOVIS image of the region from which a tomographic tilt-series was obtained at the interface between viable and cornified epidermis. (B) Overlay of the surface-rendered tomographic 3D-reconstruction (*green*) with the zero-tilt TOVIS original data (*grey*). (C) Enlargement of the tomographic 3D-reconstruction in (B). Invaginations of the plasma membrane (*green*) can be seen in association with sections of elongated tubular-like structures (*green*). Both invaginations and tubular-like structures partly contain stacks of lamellar structures (*blue stacks*) with dimensions compatible with stacked lipid bilayers. *Black dots* in (A) and (B) represent 10-nm quantum dots (PbS) used as fiducial markers for alignment of the tilt series images during 3D-reconstruction. *White dotted line* in (B) marks the interface between viable and cornified epidermis. *White asterisk* in (A): lamellar body-like structures; *Black asterisk* in (A): membrane complexes associated with ribosome complex-like structures; *White box* in (A): area shown enlarged in Fig. S2A[1]; SC in (A): stratum corneum; SG in (A): stratum granulosum; Defocus: –2 µm; *Scale bar* in B: 500 nm.

Low-intensity cellular regions, corresponding to lipid-rich material, formed a continuous tubular network expanding throughout the cell cytoplasm and were continuous with the extracellular space, to approximately 5-nm resolution (Fig. 3; Movie SII[1] FS_SET.mov).

The median diameter of the tubular network was 35 nm (range 5–165 nm; $n = 322$). Several tubular networks were identified (Fig. 3 and Movie SII[1] FS_SET.mov).

No discrete vesicular structures were observed in any 3D-reconstructed sample. TransGolgi networks associated with the extracellular space were identified in the FS-SET data (Fig. S1C[1]). Stacked lamellar material as well as multi-granular material was not resolved in the FS-SET 3D-reconstruction.

Focused ion beam scanning electron microscopy tomography

Two FIB-SEM tomograms were obtained, each with a skin sample volume of approximately $10{,}000 \times 5{,}000 \times 1{,}000$ nm^3.

Low-intensity cellular regions, corresponding to lipid-rich material, formed a large continuous tubular network expanding throughout the cell cytoplasm and were continuous with the extracellular space (Fig. 4; Movie SIII[1] FIB_SEM.mov).

The median diameter of the tubular network was 70 nm (range 40–230 nm; $n = 270$). At the approximately 40-nm resolution level (i.e. 2× the FIB milling section thickness of 20 nm), continuity of the tubular network of adjacent cells was observed occasionally (Fig. 4; Movie SIII[1] FIB_SEM.mov).

No discrete lamellar body structures were observed in any 3D-reconstructed sample. Stacked lamellar material as well as multi-granular material was not resolved in the FS-SET 3D-reconstruction.

DISCUSSION

A better knowledge of the skin barrier formation process is called for to understand the development of barrier-deficient skin disease (2). A key question is related to the topology of the SG cells' lipid secretory system (the lamellar body system (8, 25)), and the consequent compartmentalization of the different physical and chemical (26) events taking place during skin-barrier formation.

The first published model suggests a multi-vesicular system (8), similar to that of synaptic vesicle fusion (13). More recently, this idea has been challenged, and lipid delivery via folding/unfolding of a single tubuloreticular membrane system has been proposed (12), but only indirectly supported experimentally (3, 18, 22, 27). Most data of the architecture of the lamellar body system has been derived from 2D electron microscopy. The question as to whether lamellar bodies are discrete vesicular structures in 3D or merely 2D representations of a single tubuloreticular membrane network thus remains open. We have addressed this question directly by visualizing the 3D architecture of the lamellar body system using 3 highly specialized and complementary 3D electron microscopy methods (TOVIS, FS-SET, FIB-SEM), and used CEMOVIS as a near-native high-resolution 2D reference. The resolution limit of CEMOVIS

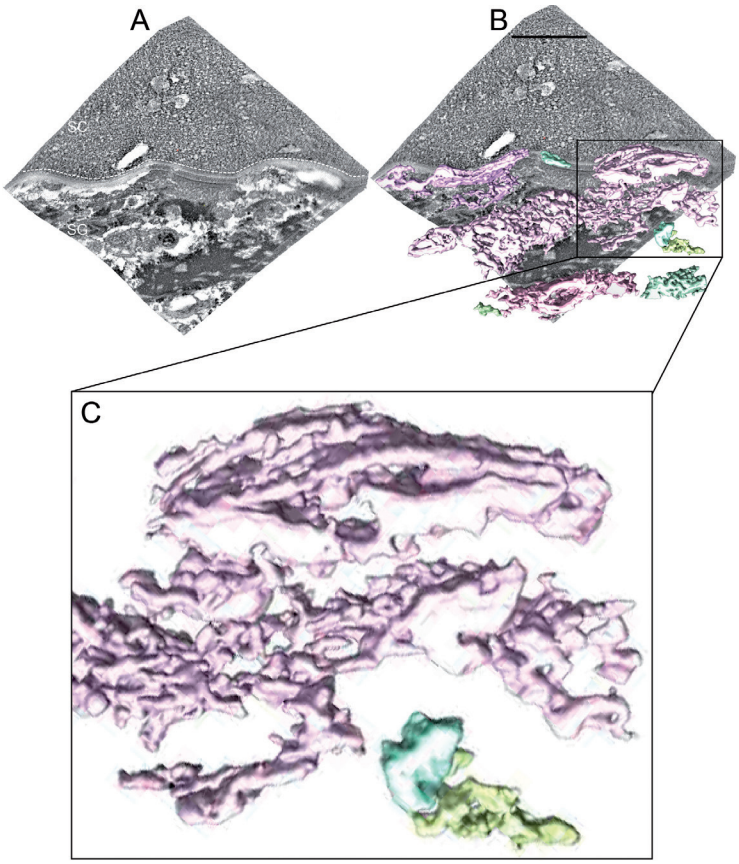

Fig. 3. Four-hundred nanometre thick freeze-substitution serial section electron tomography (FS-SET) 3D-reconstruction of the interface between viable and cornified epidermis (see Movie SII[1] FS_SET.mov). Connected structures (coloured 3D volumes in (B) and (C)) segmented out with automated watershed segmentation in a serial tomogram composed of 5 sequential dual-tilt tomograms obtained from the same area in a freeze-substituted plastic-embedded human skin sample. (A) IMOD 3D-reconstruction of the combined FS-SET data-set. (B) Overlay of surface-rendered tomographic 3D volumes obtained by watershed segmentation (*coloured 3D volumes*) with the original combined IMOD 3D-reconstructed FS-SET data-set (*grey*). (C) Enlargement of the watershed segmented 3D volume marked by a black box in (B). Note that structures that are continuous with each other in 3D are assigned the same colour by the automated watershed segmentation algorithm procedure. *White dotted line* in (A) marks the interface between viable and cornified epidermis. SC in (A): stratum corneum; SG in (A): stratum granulosum. Defocus –0.5 µm; *Scale bar* in (A): 500 nm.

is approximately 0.5 nm (1), while the resolution limit of TOVIS is approximately 2–5 nm (16), of FS-SET approximately 5 nm, and of FIB-SEM approximately 40 nm (i.e. 2 × the FIB milling section thickness of 20 nm)[2].

Our TOVIS data strongly favour the presence of tubules, not vesicles, in the near-native material (best visualized in Movie SI[1] TOVIS.avi) (Figs 2 and S2[1]; Movie SI[1] TOVIS.avi). Further ramifications and connections between the tubules themselves and between the tubules and the cell plasma membrane were clearly visualized in 3D (Figs 2 and S2[1]; Movie SI[1] TOVIS.avi), indicating the presence of a tubuloreticlar network. This is further supported by the observation that the stacked lamellar content of the tubules (Figs 2 and S2[1], and Movie SI[1] TOVIS.avi) was structurally identical with the content of the invaginations of the cell plasma membrane in widened areas of the extracellular space. Finally, no discrete vesicular structures with dimensions compatible with lamellar bodies were observed by TOVIS, FS-SET or by FIB-SEM in any of the 3D-reconstructed skin samples.

Both FS-SET (Fig. 3) and FIB-SEM (Fig. 4) showed a low-intensity tubuloreticular network with tubular dimensions varying between 5 and 230 nm protruding throughout the SG cellular space and being continuous with the extracellular space between viable and cornified epidermis. Although the membrane structures visualized with FS-SET and FIB-SEM dimensionally fit well with corresponding membrane structures visualized with CEMOVIS and TOVIS (cf. Fig. S3[1]), it cannot be excluded that membrane structures other than lamellar bodies and transGolgi networks contribute to the low-intensity signal. However, using watershed segmentation on FS-SET tomograms it was shown, to approximately 5 nm resolution, that all these membrane structures, whether defined as lamellar bodies, transGolgi networks or other membrane structures, are connected into a continuous tuboloreticular network

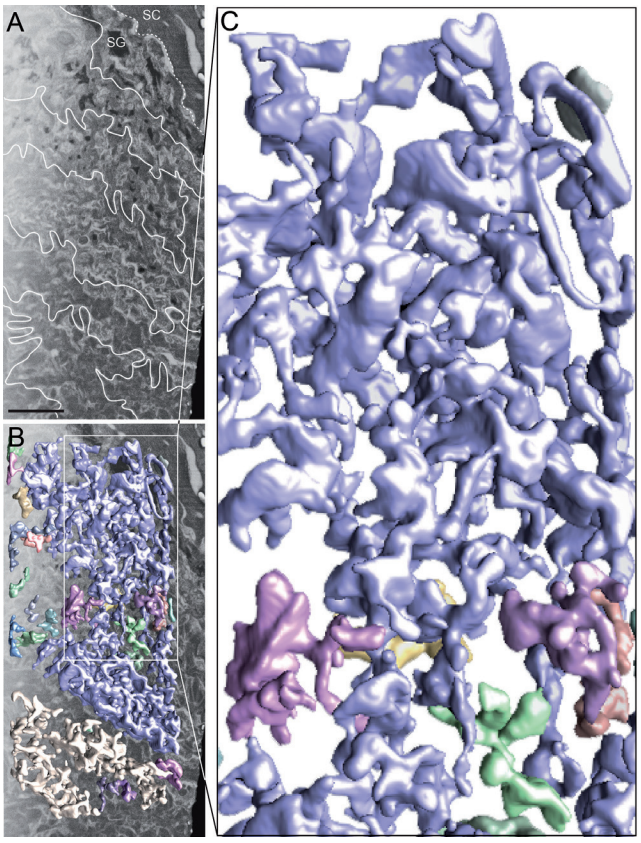

Fig. 4. One-thousand nanometre thick focused ion beam scanning electron microscopy (FIB-SEM) tomography 3D-reconstruction of the interface between viable and cornified epidermis (see Movie SIII[1] FIB_SEM.mov). Connected structures (coloured 3D volumes in (B) and (C)) segmented out with automated watershed segmentation in a 3D-reconstructed FIB-SEM tomogram. (A) Scanning electron microscopy image (SEM) of the FIB-SEM data-set composed of 50 sequential SEM images. (B) Overlay of surface-rendered tomographic 3D volumes obtained by watershed segmentation (coloured 3D volumes) with the original SEM image (*grey*) shown in (A). (C) Enlargement of the watershed segmented 3D volume marked by a *white box* in (B). Note that all structures that are continuous with each other in 3D are assigned the same colour by the automated watershed segmentation algorithm procedure. *White dotted line* in (A) marks the interface between viable and cornified epidermis. *White lines* in (A) mark the intercellular spaces in viable epidermis. SC: stratum corneum; SG: stratum granulosum. *Scale bar* in (A): 500 nm.

spanning a large portion of the cellular space and being continuous with the extracellular space between viable and cornified epidermis (Fig. 3). This finding was further supported by the FIB-SEM data in a larger volume, but at a lower resolution (Fig. 4).

FS-SET and FIB-SEM 3D-reconstructions are obtained from stained freeze-substituted skin samples, and not, as for CEMOVIS and TOVIS, directly from near-native vitreous skin samples. Therefore, influence from preparation-induced artefacts derived from solvent extraction, plastic embedding and staining cannot be excluded. However, the similar dimensions of lamellar bodies seen in TOVIS 3D-reconstructions and CEMOVIS 2D micrographs, with those seen in FS-SET projections

[2]TOVIS (16) has the advantage of high resolution and of preserving the near-native structure of skin. The epidermal tissue volume that can be studied is however limited by the thin skin section thickness (about 50 nm) needed for high-resolution work and by the method's extreme technical difficulty, not practically allowing for serial section tomography. FS-SET overcomes these problems, but preserves the skin tissue to a lesser degree than does TOVIS. Both TOVIS and FS-SET are further restricted by a limited tilt-range (about ±60–70 degrees), resulting in a smearing of the point-spread function in the section thickness dimension (16, 23). This problem is overcome by FIB-SEM that does not depend on tomographic section tilting. Another advantage is that larger tissue volumes can be 3D reconstructed than with TOVIS or FS-SET. A drawback is, however, that the resolution in the section thickness dimension is limited by the FIB slice thickness (about 20 nm). Like for FS-SET, skin tissue preservation is lower than for TOVIS. In addition to the 3D methods listed above, we used cryo-electron microscopy of vitreous sections (CEMOVIS) for obtaining 2D electron micrographs of the interface between stratum granulosum and stratum corneum, to serve as near-native very high-resolution references for the 3D reconstructions performed with TOVIS, FS-SET and FIB-SEM.

and in FIB-SEM micrographs, respectively (Fig. S3[1]), support that possible preparation-induced artefacts may not play a major role with respect to the ultrastructure of the lamellar body system at the resolution level of FS-SET and FIB-SEM tomography (5–40 nm).

The presence of a cytoplasmic tubuloreticular membrane system represented as deep interconnected invaginations of the SG cell plasma membrane implies that skin barrier formation does not proceed via vesicular transport and fusion, as previously believed. It further implies that the extracellular space at the interface between viable and cornified epidermis may spatially be closely associated with the transGolgi network as well as with other intracellular organelle systems. Different physical and chemical events related to the formation of the skin barrier lipid matrix could thus be broadly distributed within the cell cytoplasm and still be directly associated with the extracellular space. Also, due to the continuity of the tubuloreticular membrane system, the coordination and control of the barrier formation process could be mediated by membrane dynamics (12).

A challenge for the future will be to localize spatially in 3D the different physical and chemical events controlling skin barrier formation, and thus map their 3D distribution in the SG cell, their mutual spatial relations as well as their spatial relations to the tubuloreticular membrane system. To this end, one possible experimental approach could be the use of freeze-substitution immuno-electron tomography (FS-IET) (16).

Conclusion

The lamellar body system is represented by a tubuloreticular membrane network filling out a large portion of the cytoplasm and being continuous with the plasma membrane of the outermost SG cells. This implies that the extracellular space reaches deep within the cytoplasm of SG cells, which, in turn, will have a major impact on the physical and chemical events controlling skin barrier formation at the molecular level. It further implies that skin barrier formation could be regarded as a membrane folding/unfolding process, but not as a diffusion/fusion process, at the cellular level.

ACKNOWLEDGEMENTS

The present work was made possible by generous support from the Swedish Medical Society, LEO Pharma, the Wenner-Gren Foundation, and the Welander Foundation. The Knut and Alice Wallenberg Foundation is acknowledged for support of the electron microscope facility. Molecular graphics and analyses were performed with the UCSF Chimera package. Chimera is developed by the Resource for Biocomputing, Visualization, and Informatics at the University of California, San Francisco, CA, USA (supported by NIGMS P41-GM103311). We acknowledge the service of the Core Facility for Electron Tomography at Karolinska Institutet.

REFERENCES

1. Iwai I, Han HM, den Hollander L, Svensson S, Öfverstedt LG, Anwar J, et al. The human skin barrier is organized as stacked bilayers of fully extended ceramides with cholesterol molecules associated with the ceramide sphingoid moiety. J Invest Dermatol 2012; 132: 2215–2225.
2. Elias PM, Wakefield JS. Mechanisms of abnormal lamellar body secretion and the dysfunctional skin barrier in patients with atopic dermatitis J Allergy Clin Immunol 2014; 134: 781–791.
3. Elias PM, Cullander C, Mauro T, Rassner U, Kömüves L, Brown BE, et al. The secretory granular cell: the outermost granular cell as a specialized secretory cell. J Invest Dermatol Symp Proc 1998; 3: 87–100.
4. Brody I. Intercellular space in normal human stratum corneum. Nature 1966; 209: 472–476.
5. Matoltsy AG. Membrane coating granules of the epidermis. J Ultrastruct Res 1966; 15: 510–515.
6. Lavker RM. Membrane coating granules. The fate of the discharged lamellae. J Ultrastruct Res 1976; 55: 79–86.
7. Odland GF, Holbrook K. The lamellar granules of epidermis. Curr Probl Derm 1981; 9: 29–49
8. Landmann L. Epidermal permeability barrier. transformation of lamellar granule disks into intercellular sheets by a membrane-fusion process, a freeze-fracture study. J Invest Dermatol 1986; 87: 202–209.
9. Brody I. A light electron microscopy study of normal human stratum corneum with particular reference to the intercellular space. Uppsala J Med Sci 1989; 94: 29–45.
10. Fartasch M. Epidermal barrier disorders of the skin. Microsc Res Tech 1997; 38: 361–372.
11. Madison KC, Sando GN, Howard EJ, True CA, Gilbert D, Swartzendruber DC, et al. Lamellar granule biogenesis. A role for ceramide glycosyltransferase, lysosomal enzyme transport, and the Golgi. J Invest Dermatol Symp Proc 1998; 3: 80–86.
12. Norlén L. Skin barrier formation: the membrane folding model. J Invest Dermatol 2001; 117: 823–829.
13. Südhof TC. Neurotransmitter Release: the last millisecond in the life of a synaptic vesicle. Neuron 2013; 80: 675–690.
14. Masich S, Östberg T, Norlén L, Shupliakov O, Daneholt D. A procedure to deposit fiducial markers on vitreous cryo-sections for cellular tomography. J Struct Biol. 2006; 156: 461–468.
15. Norlén L, Masich S, Goldie KN, Hoenger A. Structural analysis of vimentin and keratin intermediate filaments by cryo-electron tomography. Exp Cell Res 2007; 313: 2217–2227.
16. Norlén L, Öktem O, Skoglund U. Molecular cryo-electron tomography of vitreous tissue sections: current challenges. J. Microscopy 2009; 235: 293–307.
17. De Winter DAM, Sneijdenberg CTWM, Lebbink MN, Lich B, Verkleij AJ, Drury MR, et al. Tomography of insulating biological and geological materials using focused ion beam (FIB) sectioning and low-kV BSE imaging. J Microsc 2009; 223: 372–383.
18. Norlén L, Al-Amoudi A, Dubochet J. A cryo-transmission electron microscopy study of skin barrier formation. J Invest Dermatol 2003; 120: 555–560.
19. Norlén L, Al-Amoudi A. Stratum corneum keratin structure, function, and formation: the cubic rod-packing and membrane templating model. J Invest Dermatol 2004; 123: 715–732.
20. Al-Amoudi A, Norlén L, Dubochet J. Cryo-electron microscopy of vitreous sections of native biological cells and

tissues. J Struct Biol 2004a; 148: 131–135.
21. Al-Amoudi A, Chang J-J, Leforestier A, McDowall A, Salamin LM, Norlen LPO, et al. Cryo-electron microscopy of vitreous sections. EMBO J 2004b; 23: 3583–3588.
22. Al-Amoudi A, Dubochet J, Norlén L. Nanostructure of the epidermal extracellular space as observed by cryo-electron microscopy of vitreous sections of human skin. J Invest Dermatol 2005; 124: 764–777.
23. Mastronarde DN. Dual-axis tomography: an approach with alignment methods that preserve resolution. J Struct Biol 1997; 120: 343–352.
24. Dubochet J, Satori Blanc N. The cell in absence of aggregation artifacts. Micron 2001; 32: 91–99.
25. Hayward AF. Membrane-coating granules. Int Rev Cytol 1979; 59: 97–127.
26. Raymond A-A, Gonzales de Peredo A, Stella A, Ishida-Yamamoto A, Bouyssie D, Serre G, et al. Lamellar bodies of human epidermis: proteomics characterization by high throughput mass spectrometry and possible involvement of CLIP-170 in their trafficking/secretion. Mol Cell Proteomics 2008; 7: 2151–2175.
27. Ishida-Yamamoto A, Simon M, Kishibe M, Miyauchi Y, Takahashi H, Yoshida S, et al. Epidermal lamellar granules transport different cargoes as distinct aggregates. J Invest Dermatol 2004; 122: 1137–1144.
28. Kremer JR, Mastronarde DN, McIntosh JR. Computer visualization of three-dimensional image data using IMOD. J Struct Biol 1996; 116: 71–76.
29. Pintilie GD, Zhang J, Goddard, TD, Chiu W, Gossard DC. Quantitative analysis of cryo-EM density map segmentation by watershed and scale-space filtering, and fitting of structures by alignment to regions. J Struct Biol 2010; 170: 427–438.
30. Pettersen EF, Goddard TD, Huang CC, Couch GS, Greenblatt DM, Meng EC, et al. UCSF Chimera – a visualization system for exploratory research and analysis. J Comput Chem 2004; 25: 1605–1612.
31. Schneider CA, Rasband WS, Eliceiri KW. NIH Image to ImageJ: 25 years of image analysis. Nat Methods 2012; 9: 671–667
32. Duchon CE. Lanczos filtering in one and two dimensions. J Appl Meteor 1979; 18: 1016–1022.
33. Ikeda H, Ichikawa A, Ichikawa M. The effects of freeze-substitution media on the infrastructure of inclusion bodies in type II pneumocytes of mouse lung processed by the cryofixation method. J Electron Microsc 1984; 33: 242–247.
34. Weibull C, Christiansson A. Extraction of proteins and membrane lipids during low temperature embedding of biological material for electron microscopy. J Microsc 1986; 142: 79–86.
35. Hanaich T, Sato T, Iwamoto T, Malavasi-Yamashiro J, Hoshino M, Mizuno N. A stable lead by modification of Sato's method. J Electron Microsc (Tokyo) 1986; 35: 304–306.
36. Gilbert PFC. Iterative methods for the three-dimensional reconstruction of an object from projections. J Theor Biol 1972; 36: 105–117.